Deep Electrical Investigations in the Long Valley Geothermal Area, California

WILLIAM D. STANLEY, DALLAS B. JACKSON, AND ADEL A. R. ZOHDY

U.S. Geological Survey, Denver, Colorado 80225

Direct current resistivity and time domain electromagnetic techniques were used to study the electrical structure of the Long Valley geothermal area. A resistivity map was compiled from 375 total field resistivity measurements. Two significant zones of low resistivity were detected, one near Casa Diablo Hot Springs and one surrounding the Cashbaugh Ranch–Whitmore Hot Springs area. These anomalies and other parts of the caldera were investigated in detail with 49 Schlumberger dc soundings and 13 transient electromagnetic soundings. An extensive conductive zone of 1- to 10-Ωm resistivity was found to be the cause of the total field resistivity lows. Drill hole information indicates that the shallow parts of the conductive zone in the eastern part of the caldera contain water of only 73°C and consist of highly zeolitized tuffs and ashes in the places that were tested. A deeper zone near Whitmore Hot Springs is somewhat more promising in potential for hot water, but owing to the extensive alteration prevalent in the caldera the presence of hot water cannot be definitely assumed. The resistivity results indicate that most of the past hydrothermal activity, and probably most of the present activity, is controlled by fracture systems related to regional Sierran faulting.

INTRODUCTION

Geological, hydrological, geochemical, and geophysical studies have been completed in the Long Valley geothermal area and are reported in this special issue. This paper describes the results of electrical geophysical studies using dc resistivity and time domain electromagnetic methods. The goals for this electrical geophysical study were (1) to provide additional information on the geology and the structure of the Long Valley caldera, (2) to outline conductivity anomalies possibly caused by thermal effects, (3) to aid in test hole siting, and (4) to evaluate the overall hydrothermal potential of the caldera hot-water system.

Both dc and electromagnetic methods have been used extensively in geothermal areas [*Duprat*, 1970; *Meidav*, 1970; *Cheng*, 1970; *Zohdy et al.*, 1973; *Stanley et al.*, 1973; *Jackson*, 1973; *Risk et al.*, 1970]. Depending upon the geologic environment, rock resistivities in a hydrothermal system may be decreased by several orders of magnitude because of a combination of factors:

1. Increased temperature causes lowered resistivities because of increased ionic mobility.
2. Increased temperature generally causes more dissolved solids to occur in the rock fluids, lower resistivities resulting because of increased ionic concentrations.
3. Hydrothermal alteration, mainly the formation of clays and zeolites, provides higher ionic exchange capabilities.
4. Solution activity generally increases porosity and permeability in consolidated rocks, the rock resistivities thus being decreased. However, at the upper boundaries of a convecting system, precipitation of silicates and other dissolved solids may result in large thicknesses of an impermeable precipitate of high resistivity.

Steam phase zones or mixed phase zones may depart from the general rule of lowered resistivities in a hydrothermal system.

SURVEY METHODS

Total field resistivity measurements. In order to compile a resistivity map of the caldera representing rock resistivity down to 1–2 km, bipole-dipole mapping techniques [*Zohdy*, 1973] were used. In this application a long (3–5 km) grounded wire was used to transmit a square wave with frequencies from 0.035 to 0.14 Hz and amplitudes of up to 50 A at 600–800 V. The electric field was measured by using two quasi-orthogonal measurement dipoles at dipole stations surrounding the bipole, bipole center to dipole center separations of up to 16 km being used. The electric field E along one dipole is the potential difference divided by the dipole length. The bipole-dipole array used for these studies is illustrated in Figure 1. The current bipole is shown as AB, and the measurement dipoles as MN and MN'. In addition, measurement may be made along NN'. The total electric field E is resolved from the measured components as shown in the polar plot in the upper right portion of the figure. A measure of the accuracy of the total electric field determination is provided by the size of the triangle which is formed by the projection of the three components. The measurement of three components instead of two is particularly useful when one of the two normally measured components is very small or the sign and angle between the two components means that neither component is nearly as large as the total field, a situation conducive to large errors in computation.

The simple total field resistivity [*Zohdy*, 1973] is determined from the equation

$$\bar{\rho}_E = K_{e_0} |E|/I$$

where $|E|$ is the magnitude of the total electric field, I is the input current, and K_{e_0} is the geometric factor defined by

$$K_{e_0} = \frac{\rho_0 I}{E_0} = 2\pi\left[\left(\frac{Y}{AO^3} - \frac{Y}{BO^3}\right)^2 + \left(\frac{x+L}{AO^3} - \frac{x-L}{BO^3}\right)^2\right]^{-1/2}$$

where E_0 is the electric field magnitude which would be measured over a homogeneous half space of resistivity ρ_0 with an input current of I and x, y, L, AO, and BO are as indicated in Figure 1.

Direct current soundings. Direct current vertical electrical soundings (VES) were made by using the Schlumberger array [*Keller and Frischknecht*, 1966]. Apparent resistivities for the Schlumberger array $\bar{\rho}_s$ are computed from

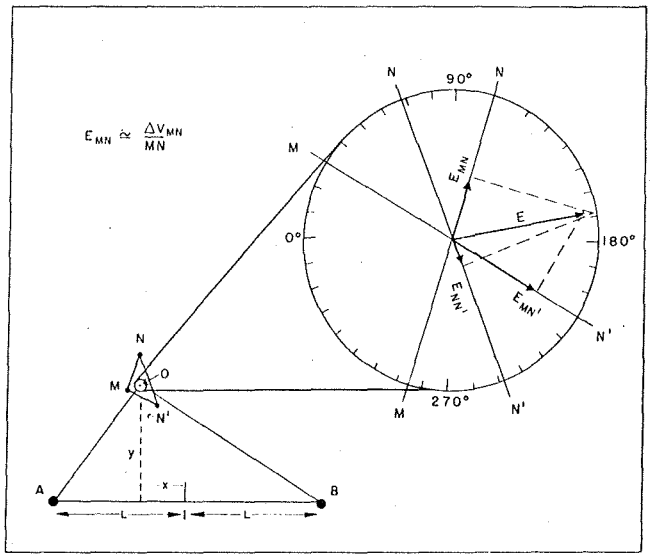

Fig. 1. Diagram of bipole-dipole array used in measuring simple total field resistivity. A and B are ground points for the bipole wire; M, N, and N' are the location of earth contact electrodes at the ends of the measurement dipoles. The polar plot in the upper right illustrates how the total field is resolved from the two or three measured components.

$$\bar{\rho}_a = \pi\left(\frac{(AB/2)^2}{MN} - \frac{MN}{4}\right)\frac{V_{MN}}{I}$$

where AB is the distance between current electrodes, MN is the distance between the potential electrodes, V_{MN} is the potential difference between the potential measuring electrodes, and I is the input current.

Time domain electromagnetic soundings. Time domain electromagnetic soundings [*Vanyan,* 1966; *Jacobson,* 1969] were made by measuring the derivative of the transient vertical magnetic field H_z caused by the current transition at the square wave input to the long grounded wire used for bipole-dipole mapping. This technique essentially measures the response of the earth to a step input. If a layered earth is assumed, information about layer thicknesses and resistivities can be obtained from the transient response. The vertical component of the transient magnetic field and the parallel component of the electric field are the most diagnostic measures of the layering parameters; however, because of induced polarization effects the electrical field measurement is less suitable than the magnetic field measurement for this type of sounding. Information about deep layers is contained mainly in the late time portion of the transient magnetic field, whereas information about the shallow layers is exhibited at early times. We denote the tran-

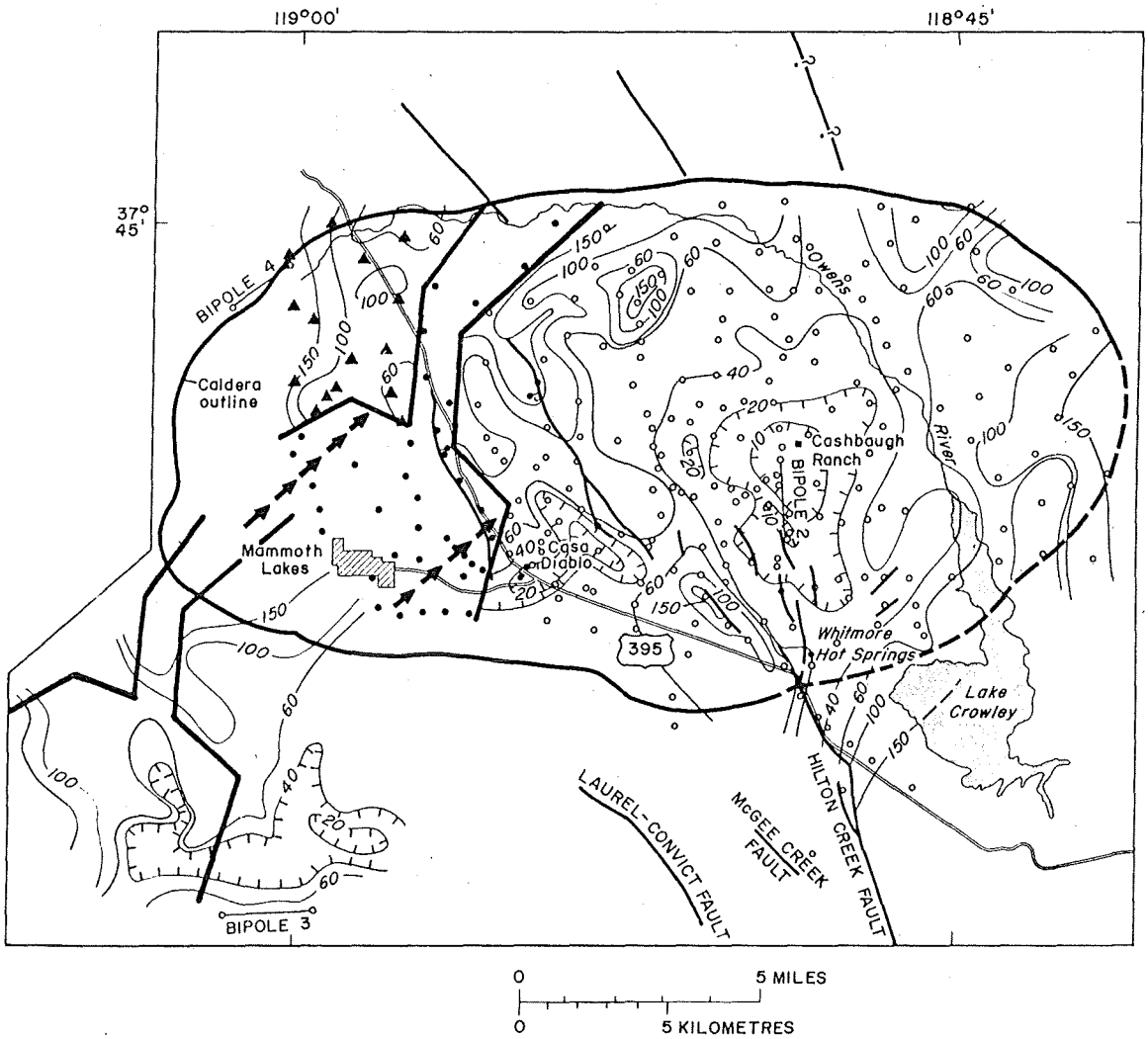

Fig. 2. Total field resistivity maps for bipole 2, 3, and 4 data. The contours for bipole 3 data have been displaced to the southwest for ease of presentation. The bold lines at the eastern margin of the bipole 4 map and at the western edge of the bipole 2 map (that define the area of the bipole 3 survey) have been reproduced on the displaced bipole 3 map to show its relationship to the other maps. Receiver stations for bipoles 2, 3, and 4 are denoted by open circles, solid circles, and solid triangles, respectively.

sient measurements described in this paper as transient magnetic soundings (TMS).

Instrumentation. The transmitter used for the bipole-dipole and TMS measurements is a square wave generator capable of an output of 80 A at 0.001–400 Hz. The square wave rise time for 3–5 km of #8 single conductor cable with a ground point resistance of 100 Ω is less than 1 ms, making it ideal for time domain electromagnetic soundings. A crystal oscillator controlling the transmitter can be synchronized with an identical oscillator in a receiver unit to provide a phase reference at the point of measurement. This phase reference was not used in synchronous detection as originally intended because a suitable detector had not been completed at the time of the survey. The phase reference was used, however, to determine the sign of the received wave form for electric field measurements and to determine time of switching for the TMS measurements.

All recording of electric fields for the bipole-dipole mapping and Schlumberger measurements was done by using strip chart recorders. Receiver dipoles were usually either 30 m or 150 m in length. The sensor for the TMS consisted of a 39-turn air core loop with an effective area of 256,000-m² turns; this loop was used to measure the derivative of the vertical component of the transient magnetic field. The voltages from the loop were amplified and recorded on a strip chart recorder after being passed through a notch filter for 60-Hz rejection.

Data Processing

Sounding data. The Schlumberger resistivity sounding data obtained in the field were adjusted to compensate for offsets caused by potential electrode spacing changes [*Kunetz*, 1966] and were smoothed to remove small cusps caused by near-surface lateral inhomogeneities [*Zohdy*, 1975]. The adjusted and smoothed curves were then digitized at six points per log cycle and processed by an automatic inversion program [*Zohdy*, 1974*c*, 1975]. The automatic program typically provides an interpretative solution of the field data consisting of seven to ten layers. Dar Zarrouk curves [*Zohdy*, 1974*a*] were then used to produce geoelectrically equivalent solutions that contained fewer layers and were correlated with nearby soundings. The final layering interpretations were checked by generating theoretical sounding curves [*Zohdy*, 1974*b*] for comparison with the field data.

Strip chart recordings of the TMS data were digitized, in terms of a time sequence of voltages, and an inverse filter was applied [*Brigham et al.*, 1968] to correct for recording system response. The resulting curves, plotted on log-log paper, were then compared with theoretical curves for a layered earth computed by using dipolar source programs developed by *Anderson* [1973] and also with curves for a finite source developed recently by W. L. Anderson (personal communication, 1974).

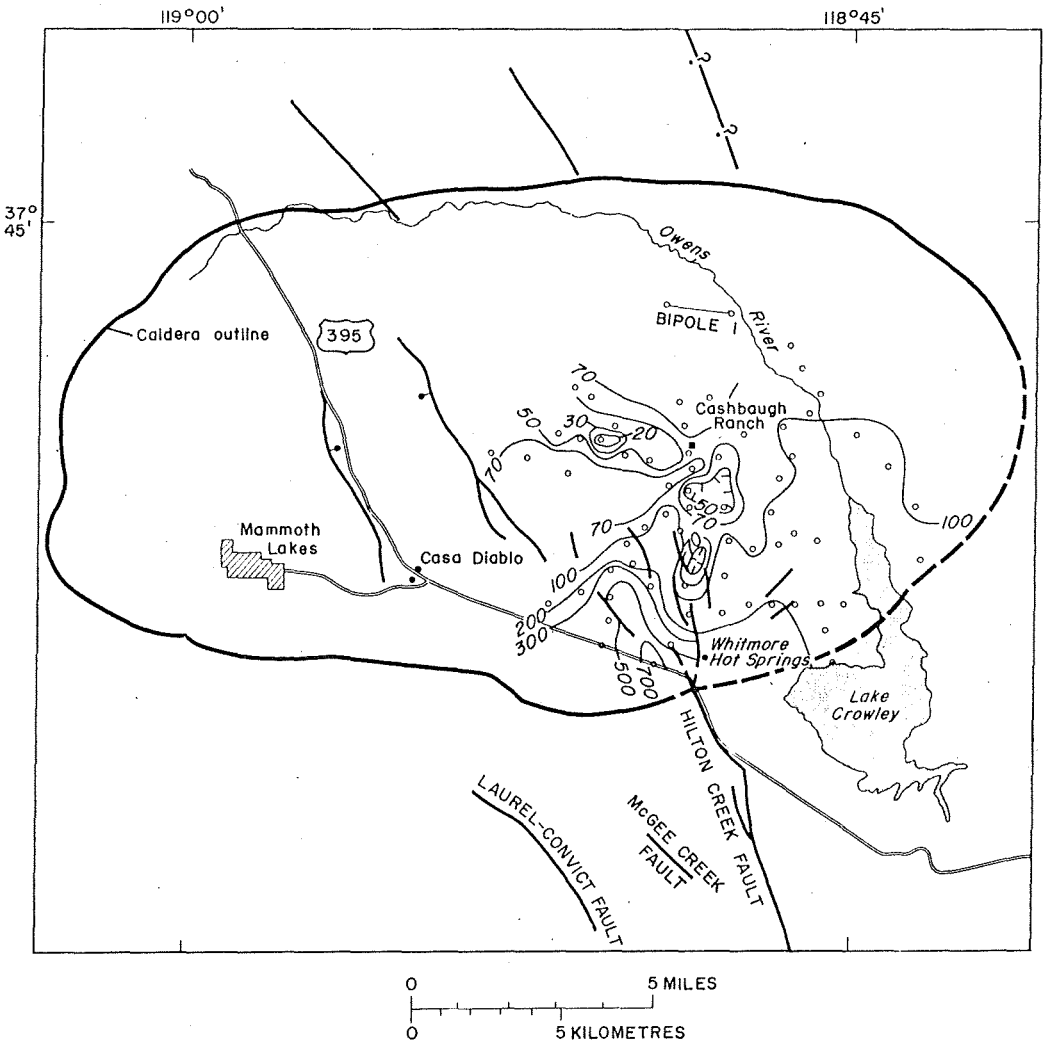

Fig. 3. Total field resistivity map for bipole 1 data. Receiver stations are denoted by open circles.

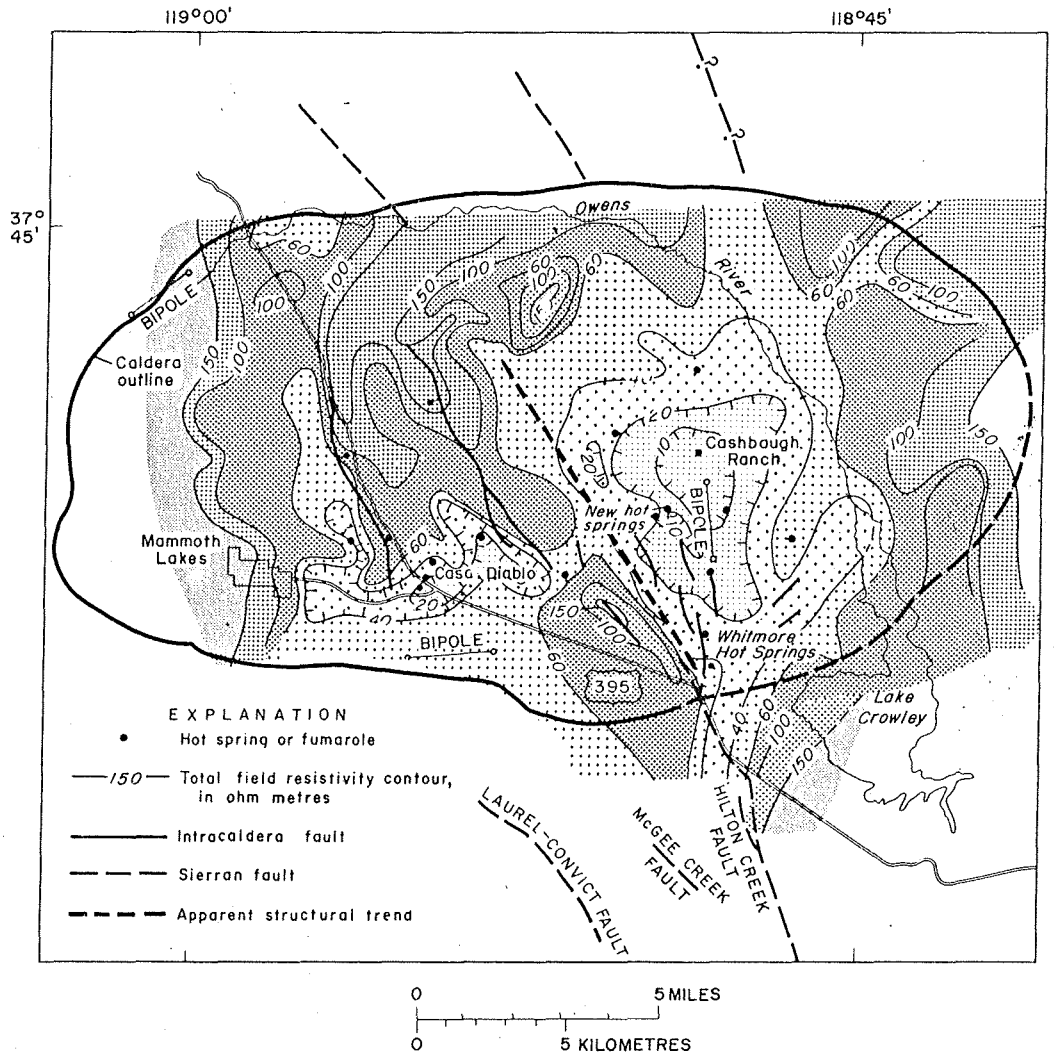

Fig. 4. Composite total field resistivity map for Long Valley caldera compiled by using data from bipoles 2, 3, and 4.

Bipole-dipole data. The total field resistivity data were processed in the field by using a programable calculator, further processing upon return from the field other than rechecking of values thus being unnecessary. The data obtained for each bipole installation were contoured for presentation in map form. Four separate apparent resistivity maps were compiled by using data from the four bipole installations. The maps for bipoles 2, 3, and 4 are shown in Figure 2, and the map for bipole 1 is shown in Figure 3. In order to compare the resistivity results with geology and other geophysical maps it was necessary to combine the four apparent resistivity maps into a single map. In considering the best method of doing this we were faced with the fact that the measured apparent resistivities about a given bipole source are a function not only of the resistivities of the geologic units in the area of the measurement but also of (1) the separation of dipole receiver and bipole transmitter, (2) the azimuth from bipole source to dipole receiver, and (3) the orientation of structures with respect to the source. Fortunately, in most geothermal areas, contrasts and physical dimensions are such that anomalies of interest are generally evident for a wide range of polarization directions and bipole-dipole separations (see, for instance, *Risk et al.* [1970] and *Stanley et al.* [1973]). This seemed to be true in Long Valley; for example, comparison of the maps for bipole 2 and bipole 3 reveals that the resistivity low near bipole 3 on that map shows up clearly on the bipole 2 map also. Comparison of the maps for bipole 1 (Figure 3) and bipole 2 (Figure 2), however (the bipole 1 stations are a subset of bipole 2 stations), indicates that the resistivity low near the bipole 2 site appears quite different on the two maps. This difference is caused by the fact that bipole 2 was inside the resistivity low, but bipole 1 was outside. Our electrical sounding interpretations show that the apparent resistivities from the bipole 2 source represent the true resistivities in the anomalous region more accurately. For this reason and because we covered most of the caldera using bipole 2, we elected to use only bipole 2, 3, and 4 data in compiling a composite map.

A synthesis of the three maps was achieved by using bipole 3 data in areas where data were not available from bipole 2 or bipole 4 and values from the latter bipoles in all other areas. The composite map (Figure 4) is the result of contouring the data values selected according to this scheme.

Interpretation of Geophysical Data

Total field resistivity map. The composite resistivity map shown in Figure 4 includes the locations of faults (modified from *Bailey et al.* [1976]) and thermal features in Long Valley, while Figure 5 provides an outcrop geology base [from *Bailey*

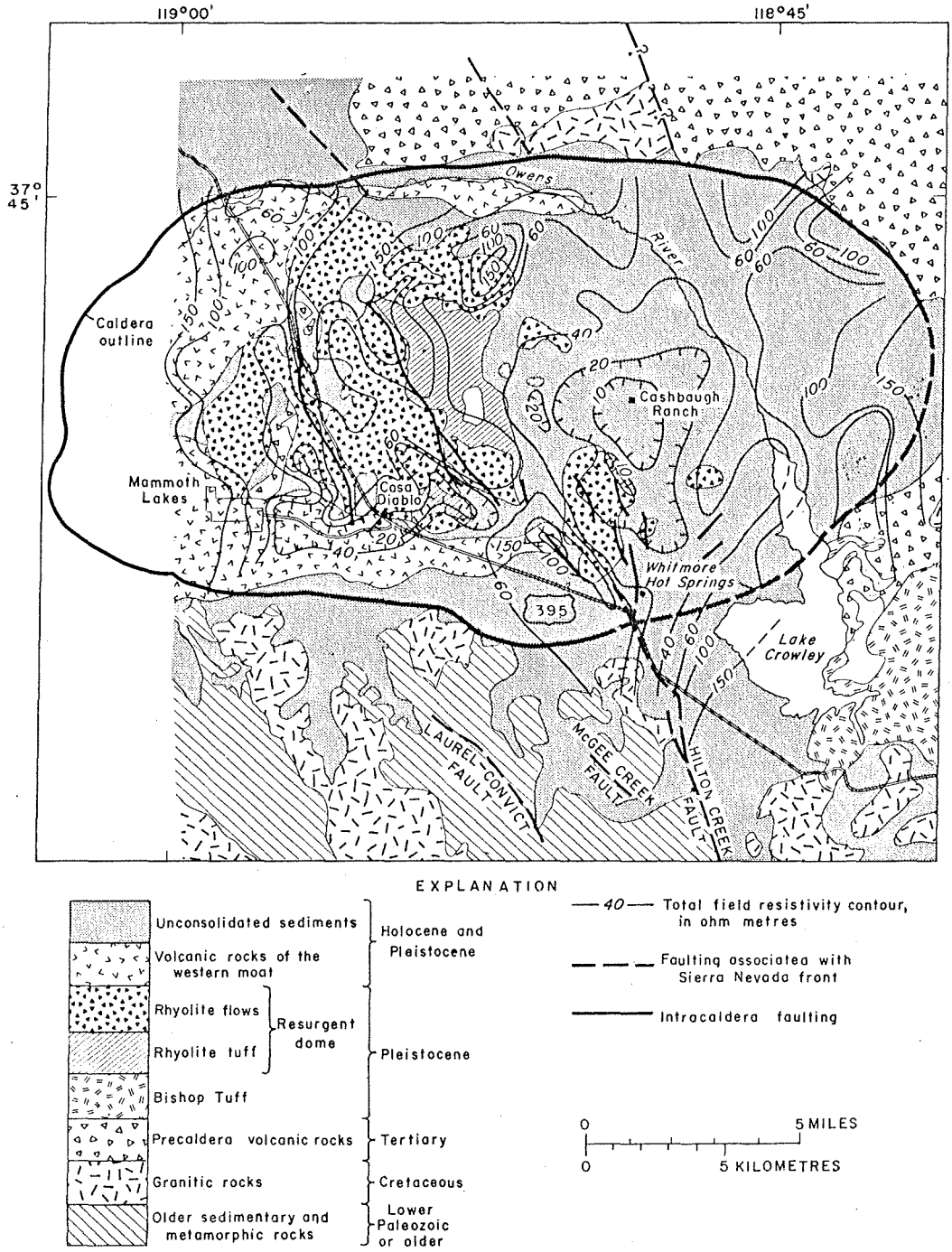

Fig. 5. Generalized geology of Long Valley caldera [after *Bailey et al.*, 1976]. Resistivity contours from this article are superimposed on the geology.

et al., 1976] for the resistivity map. The character of the total field map reveals the basic complexity of the volcanic units and hydrothermal alteration patterns within the caldera. The edge of the caldera appears to be well defined on the west, north, and east sides of the resistivity map, but on the south side the caldera boundary is not as well defined. This is probably caused by the fact that the south side of the caldera is bounded by a roof pendant of metasedimentary rocks, which are less resistive than the granodiorites that bound the structure on the other three sides.

The large volcanic centers in the resurgent dome [*Bailey et al.*, 1976] are outlined on the resistivity map by the complex of high resistivities north of Casa Diablo Hot Springs. The eastern half of the caldera is covered with unconsolidated sediments and is somewhat lower in resistivity than the western half. There are two major regions of low resistivities. The first of these is centered about the Cashbaugh Ranch area, and the second is in the region south of Casa Diablo Hot Springs.

The Cashbaugh Ranch anomaly is defined by the region with resistivities of less than 40 Ωm; however, apparent resistivities as low as 2 Ωm were measured. The anomalous region is bounded on the west by the indicated apparent structural

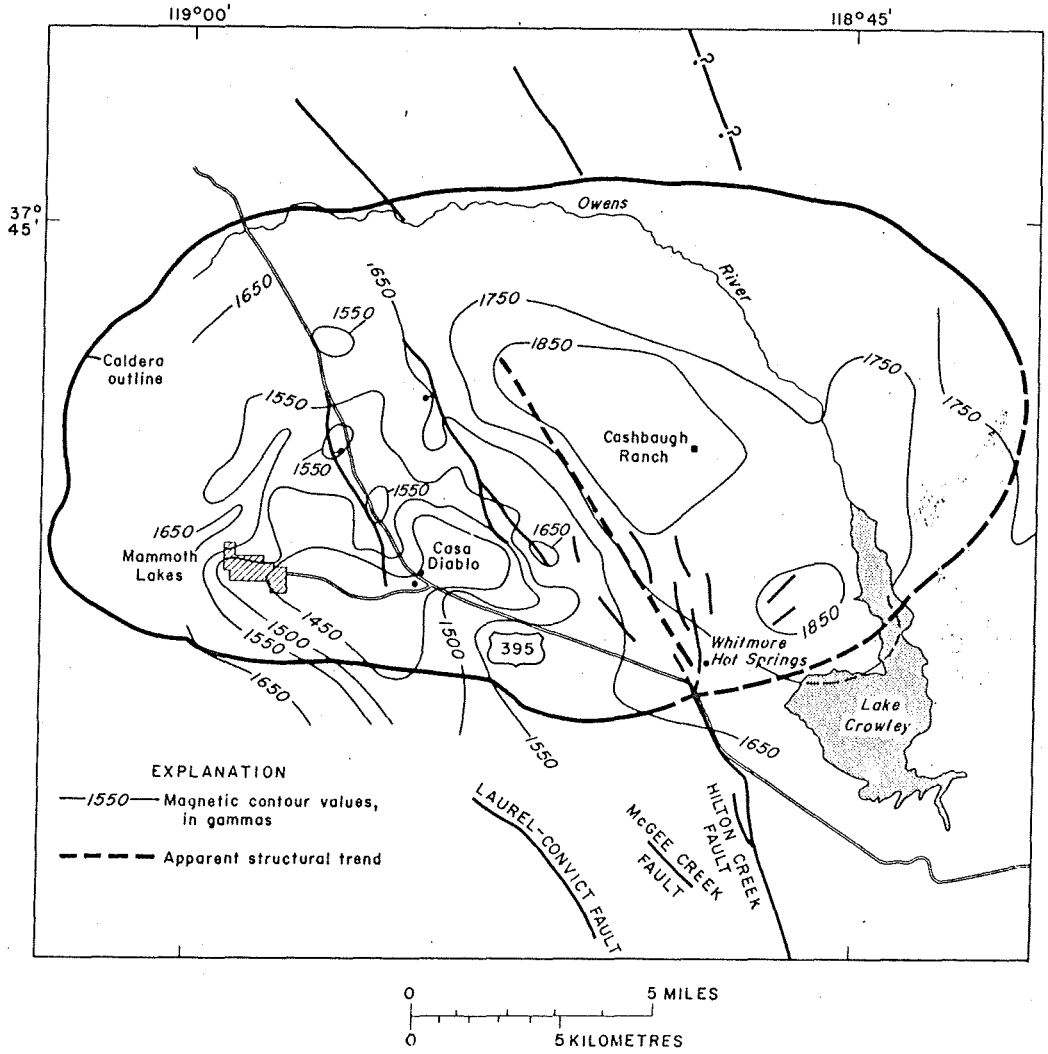

Fig. 6. Aeromagnetic map modified from *Pakiser et al.* [1964]. The map was compiled from data obtained at a flight elevation of 2.7 km.

trend, which is also evident on the aeromagnetic maps (Figures 6 and 7) and gravity map [*Kane et al.*, 1976]. On the north the resistivity anomaly appears to be truncated 2–3 km from the Cashbaugh Ranch. On the east the anomaly is truncated relatively sharply along a north-south line, and the extension of the anomaly southward into the Hilton Creek fault zone is evident. In addition to the main anomaly, there is a spur branching northeast from near the intersection of the Hilton Creek fault and the south caldera margin toward the north end of Lake Crowley. The lowest apparent resistivities were measured in a small graben southwest of Cashbaugh Ranch (small region of less than 10 Ωm aligned northwest-southeast). Several hot springs existed at the time of the survey in Hot Creek at the northwest end of this graben. Several new hot springs broke out at the northeast corner of the graben in August and October of 1973 after earthquakes occurred south and southeast of the caldera [*Bailey et al.*, 1976]. Thus the extremely low resistivities seem to indicate hot water in the highly fractured rocks of the small graben. Apparent resistivities of 2–4 Ωm were measured; therefore true resistivities are probably lower than this.

The second resistivity low is centered slightly south of Casa Diablo Hot Springs and is defined by the region with resistivities of less than 40 Ωm. The main part of the low trends in a roughly east-west direction but has a northwest-southeast pendant on the east end and an extension on the west following the keystone graben western boundary fault northward for several kilometers. These features of the anomaly shape may be representative of a ring fracture encircling the resurgent dome. The resistivity low is coincident with an aeromagnetic low of almost identical shape (Figure 6). The aeromagnetic low is superimposed upon a broader low which passes through the western part of the caldera from south to north (Figure 7). This throughgoing low is probably caused by nonmagnetic precaldera roof pendant rocks [*Kane et al.*, 1976]. The second aeromagnetic low corresponds to a total field resistivity low upon which the Casa Diablo resistivity low is superimposed. It has been estimated by using the aeromagnetic data that the roof pendant rocks are only 1 km beneath the surface in the western margin of the caldera (D. R. Mabey, personal communication, 1974), which agrees with indications from the total field maps and from sounding interpretations. The roof pendant rocks are probably more conductive than the Sierran granodiorites. However, it is possible that hot geothermal fluids in this zone could be contributing to the low resistivities. The central part of the Casa Diablo resistivity low is probably caused by extensive alteration in a tuff unit, hot geothermal fluids, or both. The central part of the Casa Diablo

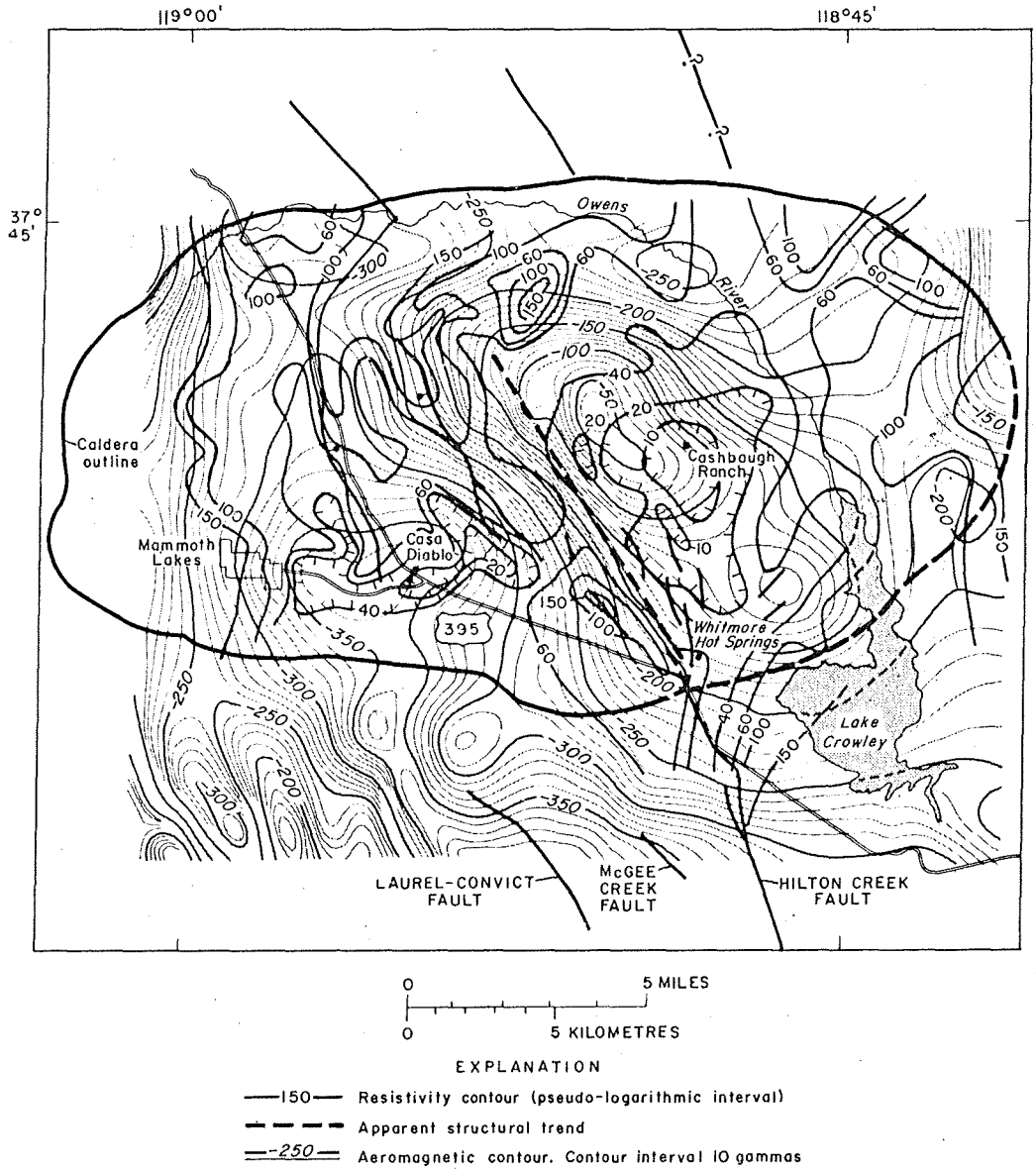

Fig 7. Aeromagnetic map from *Kane et al.* [1976] with resistivity contours from this article. The map was compiled from data obtained at a flight elevation of 4.5 km.

aeromagnetic low is probably due to hydrothermal destruction of magnetite, a phenomenon observed in hand samples from altered rhyolites around Casa Diablo Hot Springs.

Resistivity cross sections. The two main resistivity lows near Cashbaugh Ranch and Casa Diablo Hot Springs were investigated by electrical soundings to determine the probable causes of the map anomalies. Forty-nine Schlumberger VES were completed in the caldera by using maximum electrode spacings, $AB/2$, ranging from 1.22 to 3.66 km. Thirteen TMS were made by using bipoles 1 and 2.

Several resistivity cross sections were constructed from the VES and TMS interpretations, and the various electrical cross sections were used to construct a fence diagram through most of the area covered by the soundings. The locations of the fence segments, designated A–I in a clockwise direction, are shown in Figure 8 with all of the individual VES and TMS locations. In Figure 9 the fault patterns (modified from *Bailey et al.* [1976]), both regional and intracaldera, are superimposed on the fence diagram. The electrical layers may be classified as generally representing the following geologic units: (1) 1–10 Ωm, hydrothermally altered rhyolitic tuffs with both normal and high-temperature water, (2) 10- to 45-Ωm, clay-rich sediments or slightly altered rhyolitic volcanics, (3) 45- to 100-Ωm, unaltered water-saturated rhyolitic volcanics and coarse alluvium, and (4) 100- to 450-Ωm, unaltered basalt, dry volcanics, alluvial fan materials, and precaldera basement granodiorites.

A thick resistive layer at depths of 1–2 km (such as that at VES 26 on section CE) was detected on several of the soundings which are not shown on the fence diagram. This resistive layer (resistivities greater than 80–100 Ωm) is probably not precaldera basement rock but may represent the Bishop tuff, a unit which parametric VES data from outside the caldera indicate has a resistivity of about 80 Ωm. Seismic [*Hill et al.*, 1976] and gravity [*Kane et al.*, 1976] data indicate that batholith rocks are at a depth of about 3–4 km in the eastern part of the caldera.

We consider that the 1- to 10-Ωm layer generally represents rhyolitic rocks which have been extensively altered, contain large amounts of dissolved solids, and in some cases contain

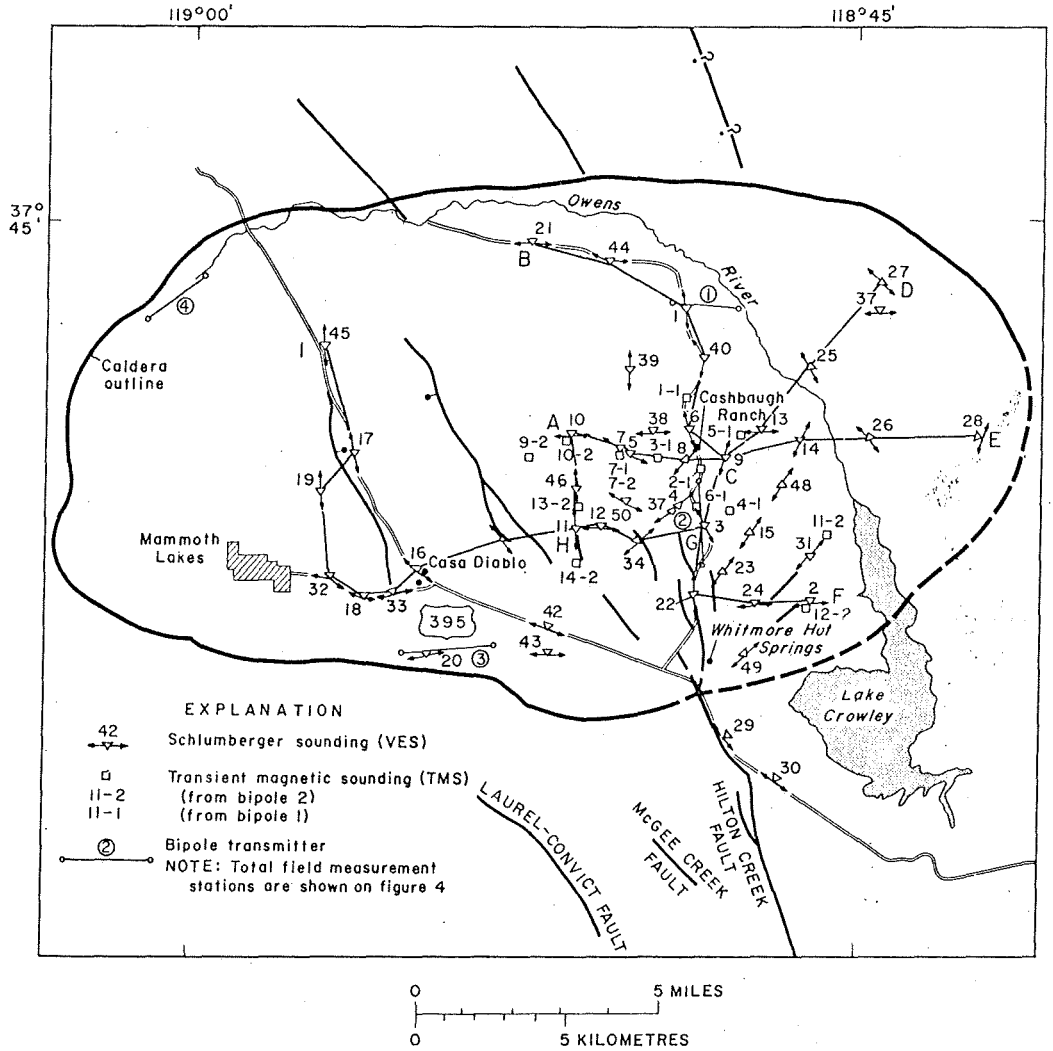

Fig. 8. Map showing location of VES and TMS and resistivity cross-section segments used in constructing the fence diagram of Figure 9. Fence segments are designated as A–I.

high-temperature water. Note that the Hilton Creek fault system has apparently been the major focus of activity along segments AC, AH, HG, CG, and GF of the fence diagram. The general attitudes and thicknesses of the conductive layer (1–10 Ωm) tend to suggest to us that the layer bears a close relationship to the occurrence of rhyolitic tuffs from sources around the resurgent dome (Figure 5). The thickening of the conductor layer along segment CGF is probably caused by a major active spur of the Hilton Creek fault passing about through points C and G. The total field resistivity low that extends from south of Whitmore Hot Springs to the north end of Lake Crowley is apparently caused by the deep conductor along segment GF.

How much of the 1- to 10-Ωm zone contains exploitable amounts of hot water is not known. It is known that wells at Casa Diablo Hot Springs have produced large amounts of hot water and steam and that considerable amounts of boiling water are issuing from the ground near the apex HGC. The only deep well data available in the eastern part of the caldera come from the U.S. Geological Survey test hole LV1, which was drilled to a depth of 300 m [*Lewis*, 1974]. The location of this test hole is shown in Figure 9, approximately midway between VES 7 and 8. The induction electrical log from LV1 was compared with pseudo-electric logs constructed from the interpretations of VES 7 and 8 (Figure 10). The VES interpretations and the interpretation of TMS 7-2, which was coincident with VES 7, were completed before the well was drilled; in fact, the well was sited to test the nature of the conductive layer. The temperature log from LV1 (Figure 10) shows a maximum temperature (at the bottom of the hole) of 73°C, certainly not indicative of a significant reservoir of hot water in this locality. Study of well cores by R. Lewis and R. Bailey (personal communication, 1974) of the U.S. Geological Survey reveals that the upper part of the hole, down to about 145 m, is in lake sediments and the remainder of the hole is in mainly rhyolitic tuffs and ashes that have been highly zeolitized by hydrothermal activity. Thus the extremely low resistivities for the conductive zone in the area of LV1 appear to have been caused by past alteration and not by the presence of hot water.

Interpretation of the true resistivity of the conductive layer was aided by the fact that TMS 7-2 was coincident with VES 7. The TMS data (Figure 11) indicated that the resistivity of the conductive layer was 1.5–3 Ωm, as the two TMS models illustrate. The model used to interpret the VES 7 data (Figure 12) agrees well with the TMS model C2 with regard to the conductive layer. The electromagnetic sounding is more sensitive to conductive layers and less sensitive to resistive layers than

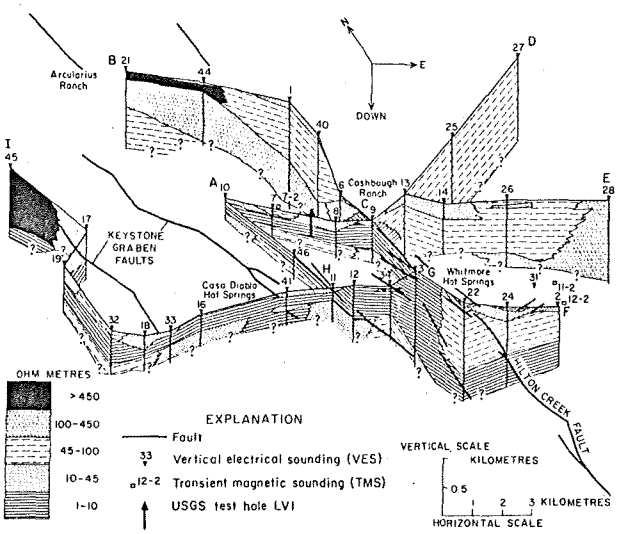

Fig. 9. Fence diagram constructed from sounding interpretations.

the VES. Therefore the models depart considerably in the shallow layers. We feel that when dc and electromagnetic sounding interpretations are combined in this way, a more accurate interpretation is obtained. This is supported by the fact that the induction log resistivities from LV1 had an average value of 2.5 Ωm for the conductive zone.

If the conductive zone (1–10 Ωm) shown in Figure 9 at Casa Diablo is due partly to highly zeolitized tuffs and partly to the presence of water up to 170°–180°C, as is indicated from the commercial wells at Casa Diablo, the effects cannot be separated. For a porous rock without clay minerals we would expect about a 250% decrease in resistivity for an increase in temperature from 73° to 180°C [*Meidav,* 1970]. However, with the high degree of alteration in the volcanics, such large resistivity differences might not be observed. The rocks in the Casa Diablo resistivity low may not be as highly altered as those near LV1, i.e., an effect from high-temperature fluids could be present but is undeterminable. Thus for all of the

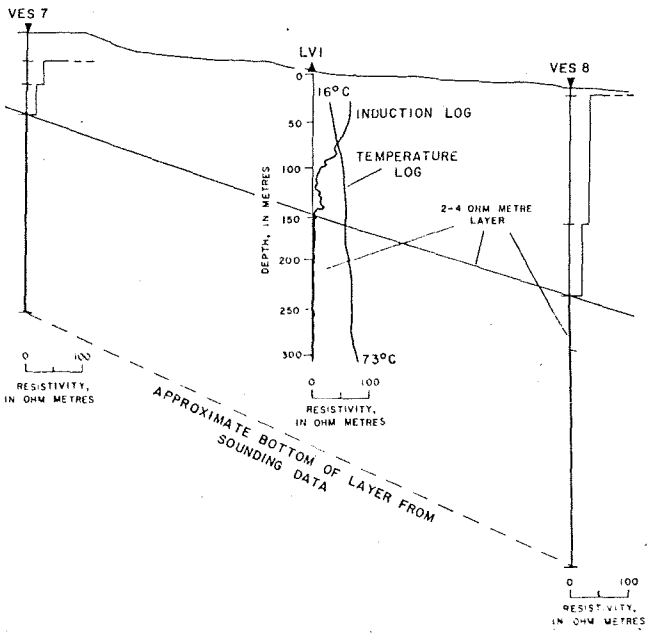

Fig. 10. Test hole LV1 temperature and induction logs with interpretations for VES 7 and VES 8.

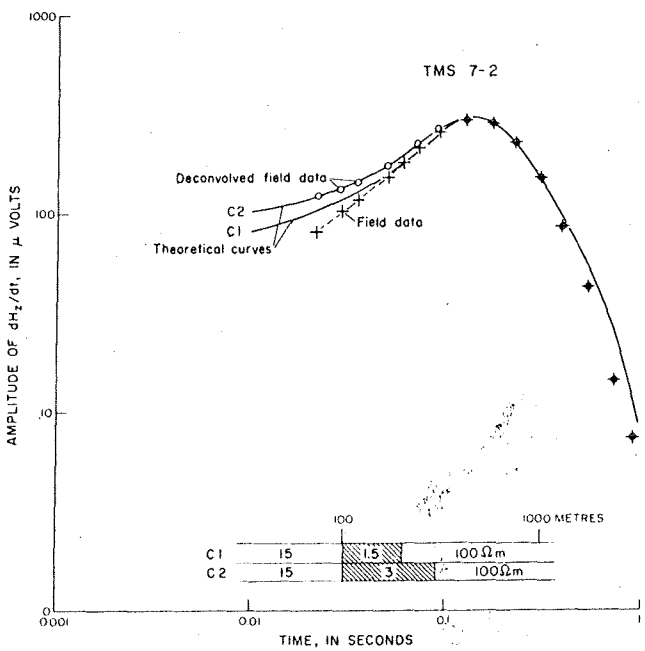

Fig. 11. Field data and interpretations for TMS 7-2. Models used for computing the theoretical curves C1 and C2 are plotted with depths along the horizontal logarithmic axis. The numbers in the model layers represent interpreted resistivity in ohm meters.

conductive zone (the 1- to 10-Ωm layer on the fence diagram) we cannot tell whether the resistivities are low owing to the presence of high-temperature fluids, alteration like that near LV1, or both.

A major question to be answered concerns the existence of deep conductors, such as the one shown on segment GF of Figure 9 at other locations in the caldera. We found no evidence in the total field data of any deep conductors except those shown on the fence diagram of the resistivity cross sections (Figure 9). Interpretation of the total field resistivity measurements as pseudo-soundings (by plotting the resistivities versus bipole-dipole center separation) were of no help in this respect because of the extreme lateral resistivity variations across the span of large bipole-dipole separations.

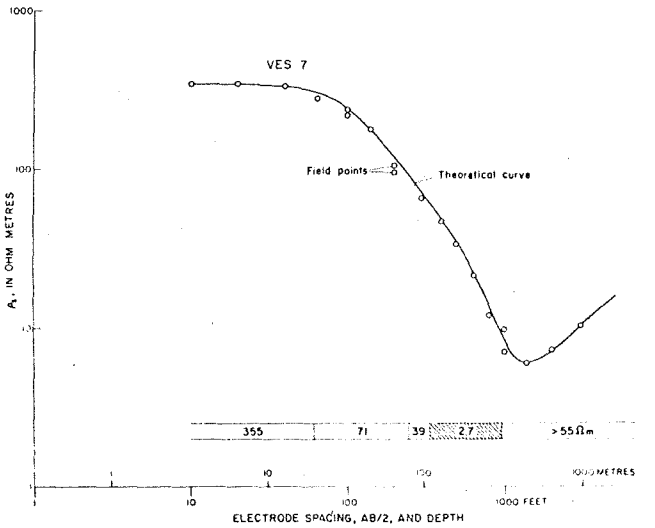

Fig. 12. Field data and interpretation for VES 7. Model used to calculate the theoretical curve is plotted with depth along the horizontal logarithmic axis, and the numbers in the model layers are interpreted resistivity in ohm meters.

Some constraints are placed upon the possibility of the existence of deep conductors, however, by the TMS data. To illustrate the effect that a conductor in the zone of 1–2 km would have upon the type of TMS data obtained in Long Valley, two model curves are presented in Figure 13. Curves A and B for models A and B show that the deep conductor has significant effect upon the TMS curve shape and the position of the asymptotic right branch. Model B in Figure 13 is modified from the model used for TMS 7-2 (Figure 11) by the addition of the deeper conductor.

From consideration of models such as those of Figure 13 we tend to rule out the possibility of extensive deep conductors in the eastern half of Long Valley (TMS data were not obtained in the western half). We do not see any evidence of major deep conductors in the TMS data other than the one on segment GF of Figure 9. From our TMS model studies we define a major conductor in Long Valley as one of at least 0.5-km thickness and less than 10-Ωm resistivity (greater than 50-mho conductance).

If major reservoirs with 150°–200°C or greater water exist in permeable rhyolitic volcanic rocks at depths less than 2 km, then we would expect them to approach our definition of major conductors (greater than 50-mho conductance) unless significant amounts of the reservoir fluids occur in a mixed phase system (steam and water). Under these assumptions a laterally extensive reservoir such as this was not detected in the electrical data in the upper 2 km.

Speculations and conclusions. The bipole-dipole resistivity, VES, and TMS data have provided a detailed picture of the electrical structure of the upper 2 km in Long Valley. These data reveal that hydrothermal activity observed at the surface and at depth by the electrical interpretations is largely controlled by fracture systems, especially those related to regional Sierran faulting. Most of the hydrothermal alteration patterns in the upper kilometer seem to be related to an ash and tuff unit flanking the resurgent dome. This conductive zone is known to contain water of only 73°C in one place (LV1) but water of up to 150°–180°C in another (Casa Diablo Hot Springs).

The only deep conductor detected which may represent a significant reservoir in the range 1–2 km is the conductive zone illustrated on segment GF of Figure 9. This zone may be representative of a reservoir in permeable volcanic rocks which is feeding the hot springs and shallow hot-water zones in this part of the caldera. The occurrence of hot water in this deep zone, if hot water is present, may be limited to the vicinity of the fractures related to the Hilton Creek fault system, as is suggested by the shape of the resistivity anomaly outlining this zone in Figure 4. This fracture system may be carrying hot water upward from depths even greater than 2 km, where the actual primary reservoir of 200°C water (suggested by geothermometric data) may occur in Long Valley. But then again the electrical anomaly may also be caused largely by extensive past hydrothermal alteration and not by the presence of high-temperature geothermal fluids. Zones in the upper 2 km of Long Valley which contain a mixed phase fluid may not have been delineated by the electrical data, although these zones may exist.

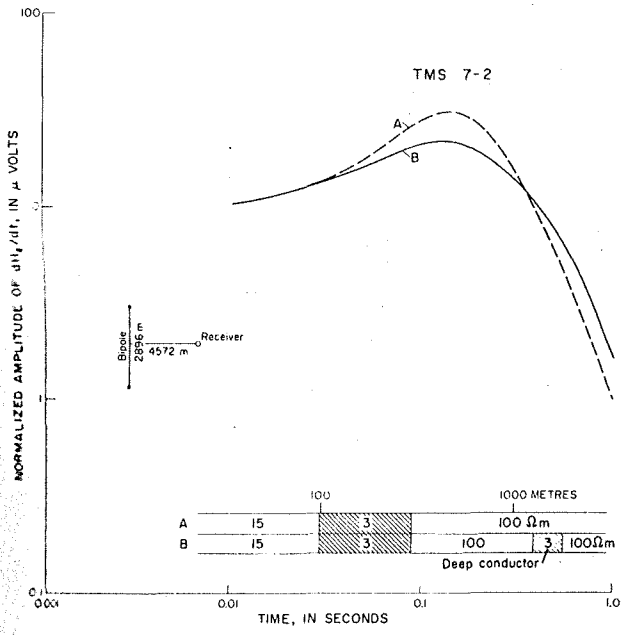

Fig. 13. Theoretical models and computed curves for TMS soundings. Model A is the model used for interpreting TMS 7-2. Model B has an additional deep conductor with a resistivity of 3 Ωm and a thickness of 500 m. Bipole length and bipole-receiver separation are shown in the lower left of the figure.

REFERENCES

Anderson, W. L., Fortran 4 programs for the determination of the transient tangential electric field and vertical magnetic field about a vertical magnetic dipole for an *n*-layer stratified earth by numerical integration and digital linear filtering, *Rep. PB2-21240,* 82 pp., Nat. Tech. Inform. Serv., Springfield, Va., 1973.

Bailey, R. A., G. B. Dalrymple, and M. A. Lanphere, Volcanism, structure, and geochronology of Long Valley caldera, Mono County, California, *J. Geophys. Res., 81*(2), this issue, 1976.

Brigham, O. E., H. W. Smith, F. X. Bostick, and W. D. Duesterhoeft, An iterative technique for determining inverse filters, *IEEE Trans. Geosci. Electron., 6*(2), 86, 1968.

Cheng, W . T., Geophysical exploration in the Tatun volcanic region, Taiwan, *Geothermics, Spec. Issue 2,* 262–274, 1970.

Duprat, A., Contribution de la géophysique à l'étude de la région géothermique de Denizle-Sararykay, Turquie, *Geothermics, Spec. Issue 2,* 275–286, 1970.

Hill, D. P., Structure of Long Valley caldera, California, from a seismic refraction experiment, *J. Geophys. Res., 81*(2), this issue, 1976.

Jacobson, J. J., Deep electromagnetic sounding technique, Ph.D. thesis, Colo. Sch. of Mines, Golden, 1969.

Jackson, D. B., Map showing percent lateral effect of total field resistivity, Marysville area, Lewis and Clark Co., Montana, open file report, U.S. Geol. Surv., Menlo Park, Calif., 1973.

Kane, M. F., D. R. Mabey, and R.-L. Brace, A gravity and magnetic investigation of the Long Valley caldera, Mono County, California, *J. Geophys. Res., 81*(2), this issue, 1976.

Keller, G. V., and F. C. Frischknecht, *Electrical Methods in Geophysical Prospecting,* p. 95, Pergamon, New York, 1966.

Kunetz, G., *DC Resistivity Methods, Geoexploration Monogr.,* The Hague, Netherlands, 1966.

Lewis, R. E., Data on wells, springs, and thermal springs in Long Valley, Mono County, California, open file report, U.S. Geol. Surv., Menlo Park, Calif., 1974.

Meidav, T., Application of electrical resistivity and gravimetry in deep geothermal exploration, *Geothermics, Spec. Issue 2,* 303–310, 1970.

Pakiser, L. C., M. F. Kane, and W. H. Jackson. Structural geology and volcanism of Owens Valley regions, California—A geophysical study, *U.S. Geol. Surv. Prof. Pap. 438,* 1964.

Risk, G. F., W. J. P. MacDonald, and G. B. Dawson, D.C. resistivity surveys of the Broadlands geothermal region, New Zealand, *Geothermics, Spec. Issue 2,* 287–294, 1970.

Stanley, W. D., D. B. Jackson, and B. C. Hearn, Jr., Preliminary results of geothermal investigations near Clear Lake, Calif., open file report, U.S. Geol. Surv., Menlo Park, Calif., 1973.

Vanyan, L. L., *Electromagnetic Depth Soundings,* translated by G. V. Keller, Consultants Bureau, New York, 1966.

Zohdy, A. A. R., Total field resistivity mapping (abstract), *Geophysics, 38*(6), 1231, 1973.

Zohdy, A. A. R., The use of Dar Zarrouk curves in the interpretation of VES data, *U.S. Geol. Surv. Bull., 1313-D,* 1974*a*.

Zohdy, A. A. R., A computer program for the calculation of Schlumberger sounding curves by convolution, *Rep. PB-232056,* Nat. Tech. Inform. Serv., Springfield, Va., 1974*b*.

Zohdy, A. A. R., A computer program for the automatic interpretation of Schlumberger sounding curves over horizontally stratified media, *Rep. PB-232703,* Nat. Tech. Inform. Serv., Springfield, Va., 1974*c*.

Zohdy, A. A. R., Automatic interpretation of Schlumberger sounding curves using modified Dar Zarrouk functions, *U.S. Geol. Surv. Bull., 1313-E,* 1975.

Zohdy, A. A. R., L. A. Anderson, and L. J. P. Muffler, Resistivity self-potential, and induced polarization surveys of a vapor-dominated geothermal system, *Geophysics, 38*(6), 1130–1144, 1973.

(Received December 23, 1974;
revised September 12, 1975;
accepted September 15, 1975.)